Electronic Supplementary Material (ESI) for Materials Chemistry Frontiers.

Electronic Supplementary Information

Photoinduced electron transfer endows fluorogenicity in tetrazine-based near-infrared labels

Tianruo Shen,[a] Xin Li,[b] and Xiaogang Liu[a,*]

a. Science, Mathematics and Technology Cluster, Singapore University of Technology and Design, 8 Somapah Road, Singapore 487372, Singapore

b. College of Pharmaceutical Science, Zhejiang University, 866 Yuhangtang Road, Hangzhou 310058, China

Corresponding author:

Xiaogang Liu: xiaogang_liu@sutd.edu.sg

Contents

1. Experimental conditions for the reported tetrazine-based labels with/toward near-infrared emissions

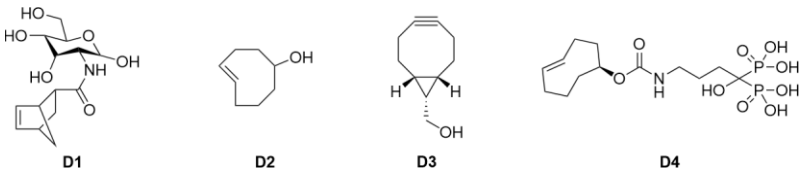

Fig. S1 Molecular structures of different dienophiles.

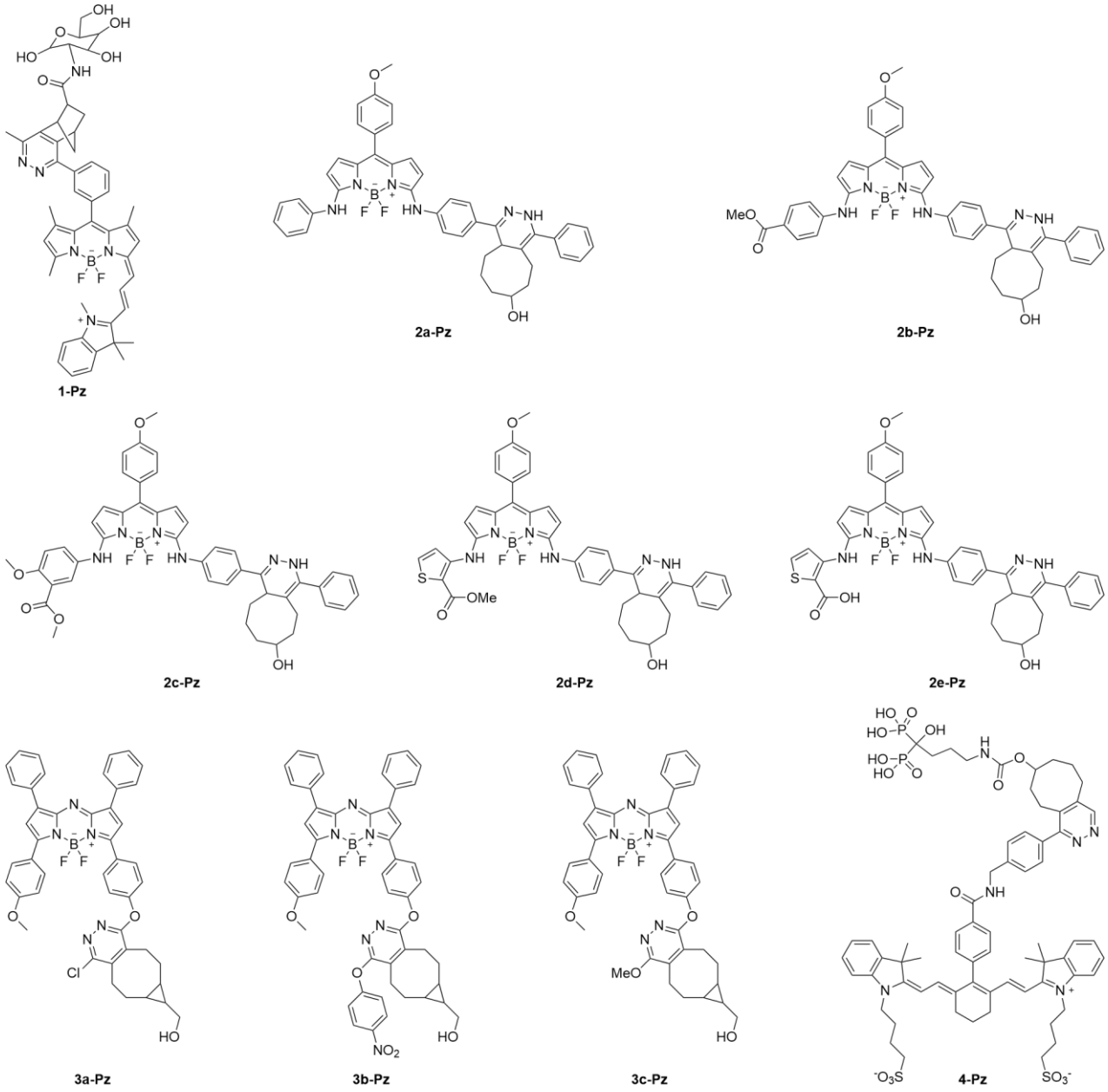

Fig. S2 Molecular structures of post-reacted labels upon inverse electron-demand Diels–Alder (iEDDA) reactions.

Table S1 Experimental conditions for four sets of labels.

Set	Reacted with	Medium	Reference
1	D1	DMF/PBS = 1:1, v/v	Xu *et al.*[1]
2	D2	DMF/PBS = 1:1, v/v	Yang *et al.*[2]
3	D3	$CHCl_3$	Wu and O'Shea[3]
4	D4	*In vivo*	Sadeghi *et al.*[4]

Table S2 Photophysical properties of different post-reacted labels.

Molecule	Maximum molar extinction coefficient (ε_{max}; $cm^{-1}\times M^{-1}$)	Quantum yield (φ)	Reference
3a-Pz	92,000	0.33	Wu and O'Shea[3]
3b-Pz	90,000	0.34	
3c-Pz	91,000	0.34	
4-Pz	150,133	0.014	Sadeghi *et al.*[4]

2. Computational methods and additional results

The density functional theory (DFT) and time-dependent DFT (TD-DFT) calculations were performed in the Gaussian 16.[5-7] All the calculations were performed using BHandHLYP functional and 6-31G** basis set.[8-10] Solvation effects were considered by deploying the Solvation Model Based on the Density (SMD) solvent model and corrected linear-response (cLR) solvent formalism.[11, 12] All the optimized molecular structures at the ground and excited states were validated at the local minimums (with positive frequencies) of the potential energy surfaces. The analyses of hole-electron distributions and frontier orbitals were conducted and visualized using Multiwfn and VMD. [13, 14]

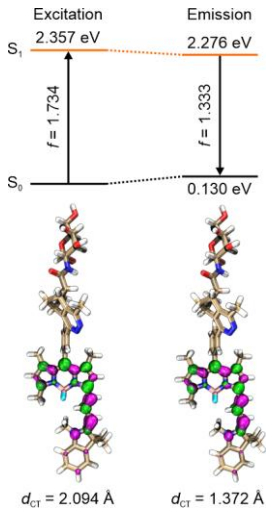

Fig. S3 Energy levels and oscillator strength (*f*) of key states with corresponding hole-electron distributions and charge transfer distance (d_{CT}) of **1-Pz** during the excitation and emission processes in DMSO. Electron: highlighted in green; Hole: highlighted in pink.

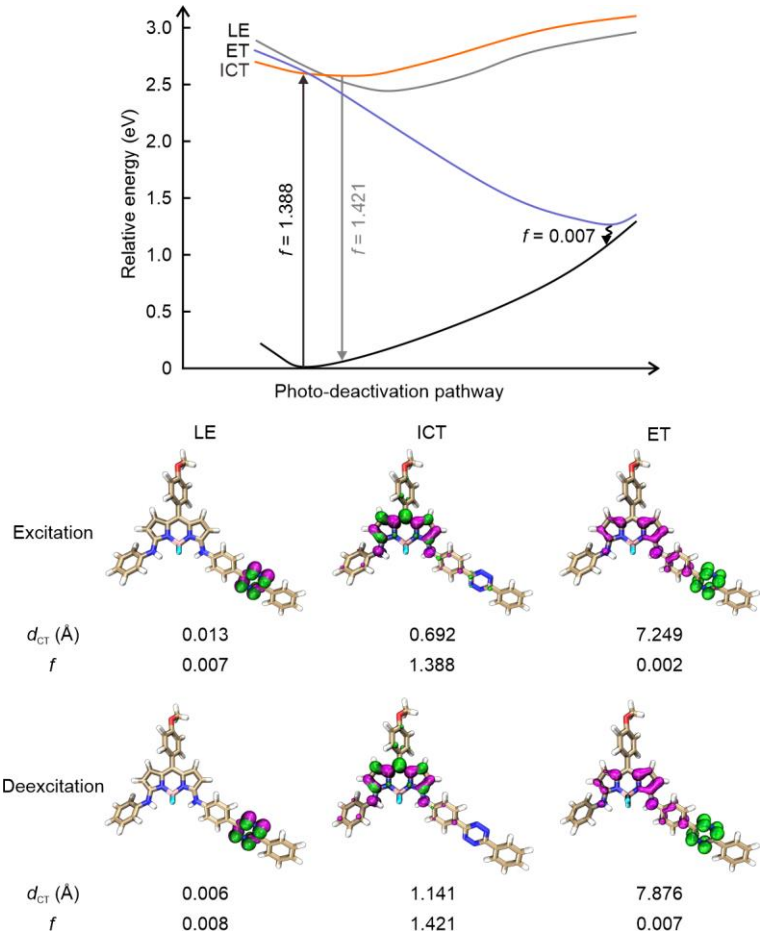

Fig. S4 Energy levels of key states with corresponding hole-electron distributions, d_{CT}, and *f* of **2a** during the excitation and deexcitation processes in DMSO. LE: locally excited; ICT: intramolecular charge transfer; ET: electron transfer; Electron: highlighted in green; Hole: highlighted in pink.

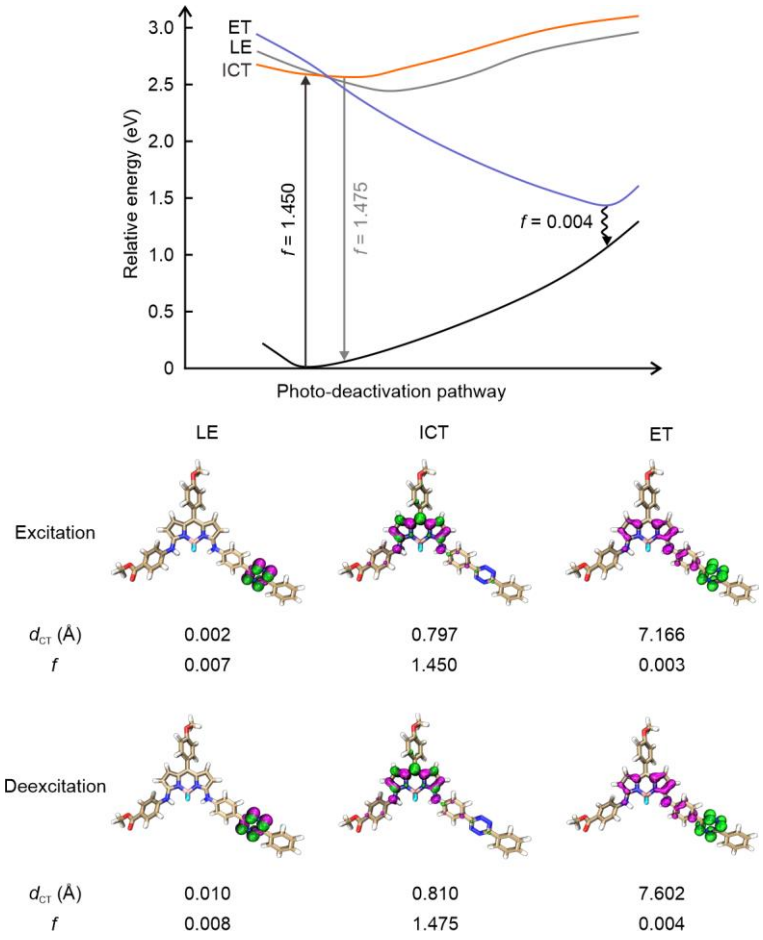

Fig. S5 Energy levels of key states with corresponding hole-electron distributions, d_{CT}, and f of **2b** during the excitation and deexcitation processes in DMSO. LE: locally excited; ICT: intramolecular charge transfer; ET: electron transfer; Electron: highlighted in green; Hole: highlighted in pink.

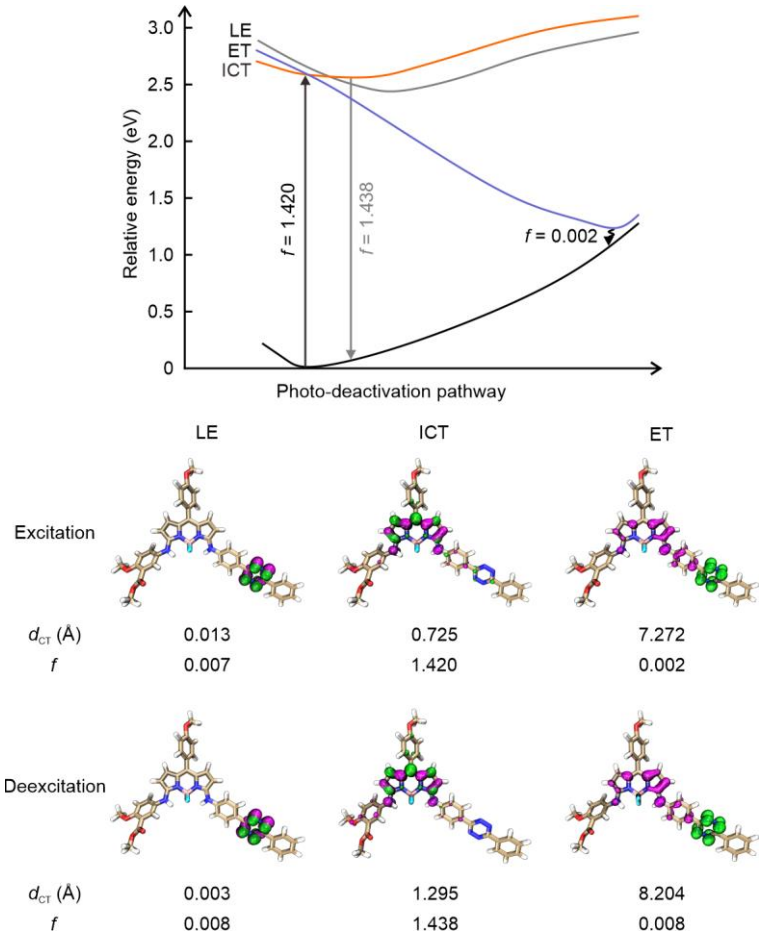

Fig. S6 Energy levels of key states with corresponding hole-electron distributions, d_{CT}, and f of **2c** during the excitation and deexcitation processes in DMSO. LE: locally excited; ICT: intramolecular charge transfer; ET: electron transfer; Electron: highlighted in green; Hole: highlighted in pink.

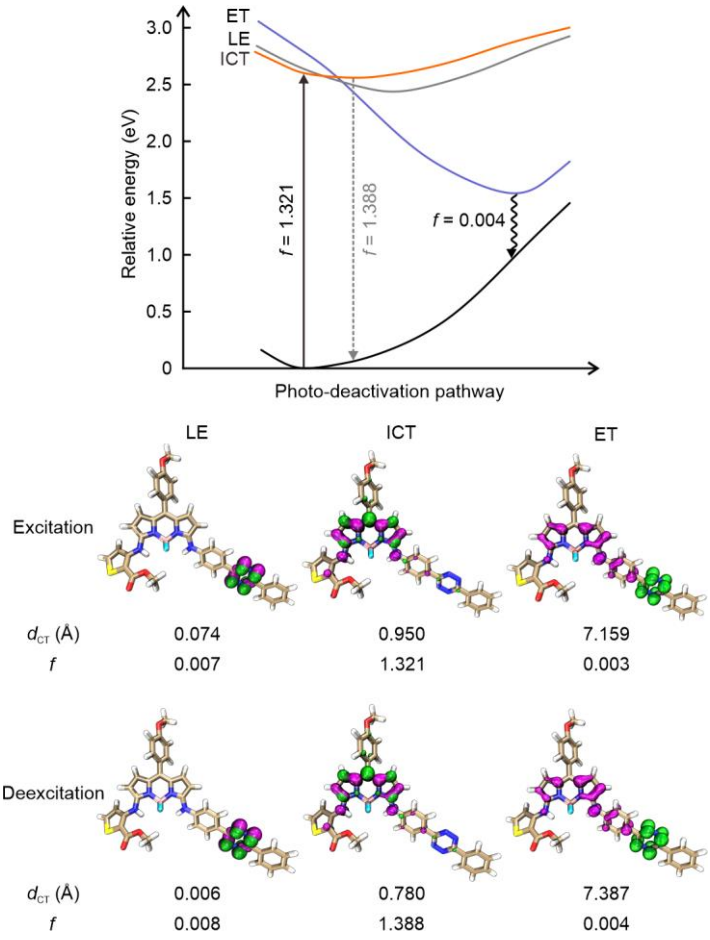

Fig. S7 Energy levels of key states with corresponding hole-electron distributions, d_{CT}, and f of **2e** during the excitation and deexcitation processes in DMSO. LE: locally excited; ICT: intramolecular charge transfer; ET: electron transfer; Electron: highlighted in green; Hole: highlighted in pink.

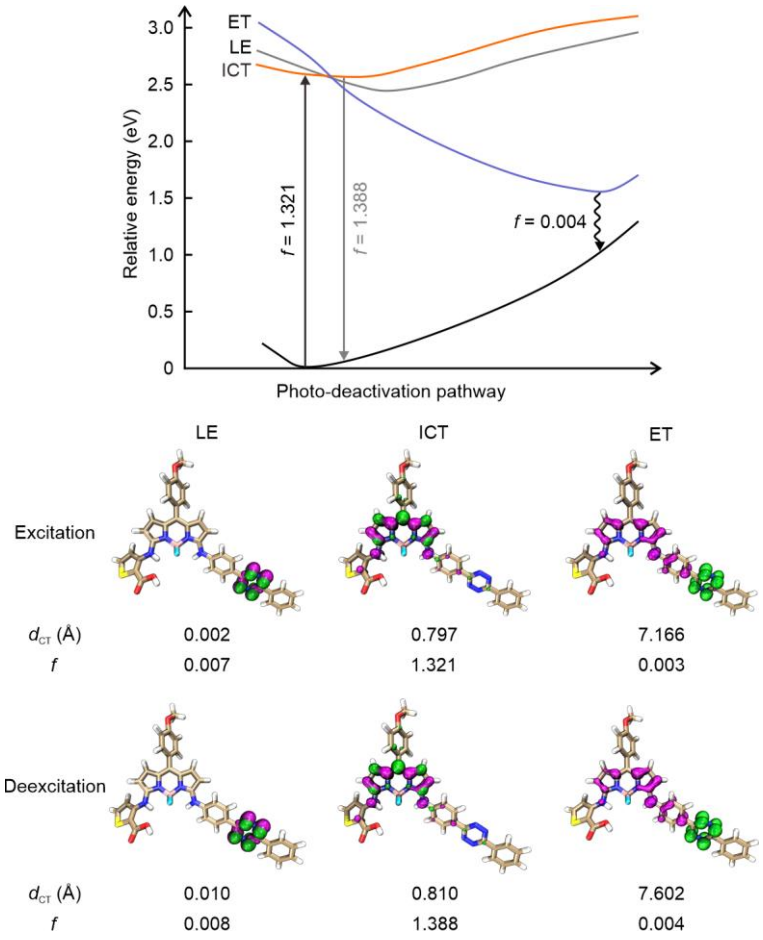

Fig. S8 Energy levels of key states with corresponding hole-electron distributions, d_{CT}, and f of **2e** during the excitation and deexcitation processes in DMSO. LE: locally excited; ICT: intramolecular charge transfer; ET: electron transfer; Electron: highlighted in green; Hole: highlighted in pink.

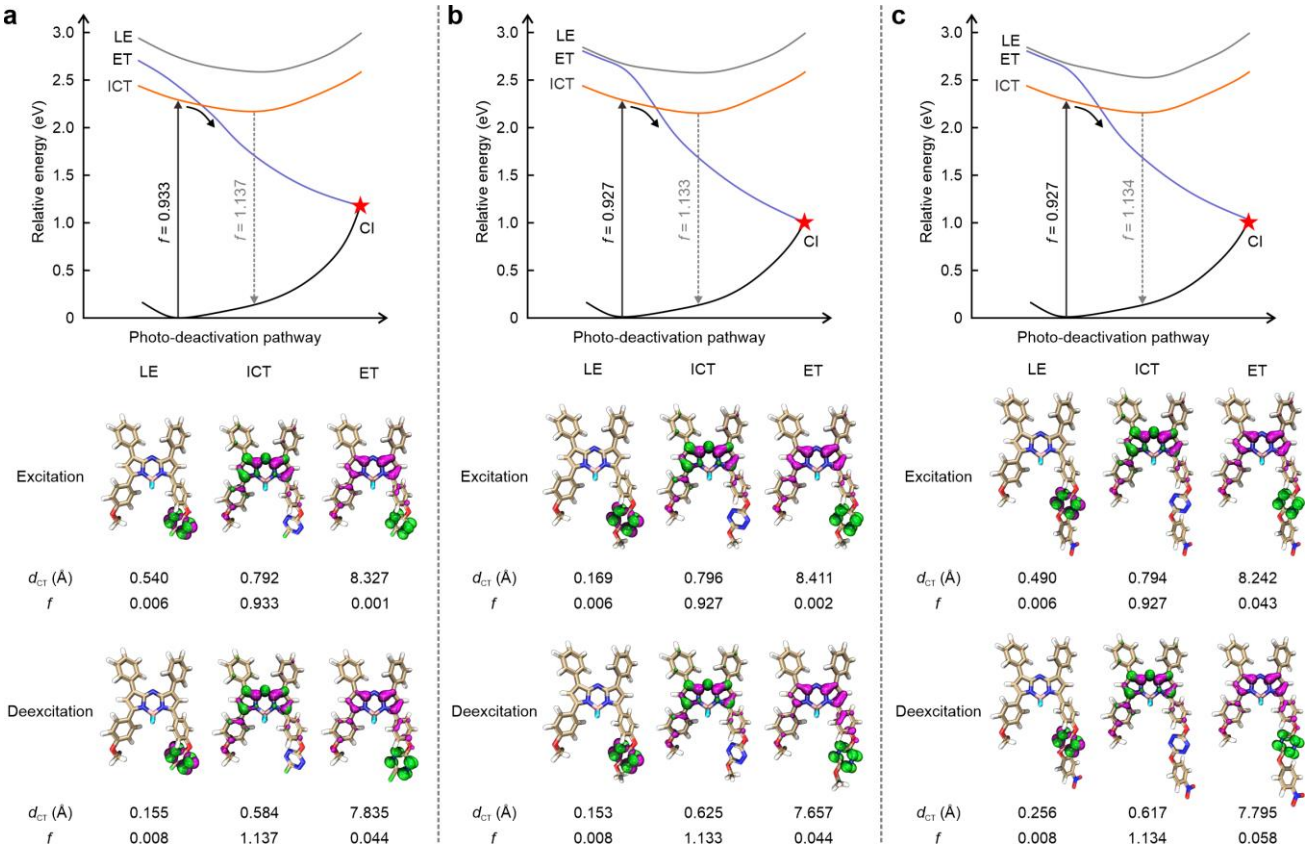

Fig. S9 Energy levels of key states with corresponding hole-electron distributions, d_{CT}, and f of (a) **3a**, (b) **3b**, and (c) **3c** during the excitation and deexcitation processes in water. LE: locally excited; ICT: intramolecular charge transfer; ET: electron transfer; Electron: highlighted in green; Hole: highlighted in pink.

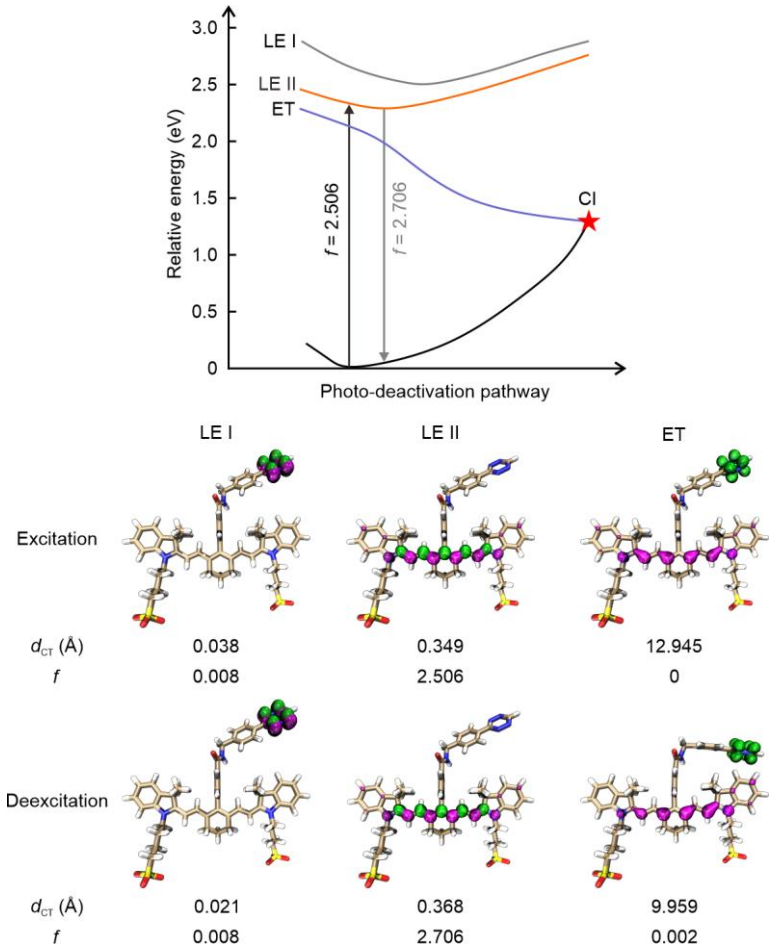

Fig. S10 Energy levels of key states with corresponding hole-electron distributions, d_{CT}, and f of **4** during the excitation and deexcitation processes in DMSO. LE: locally excited; ET: electron transfer; Electron: highlighted in green; Hole: highlighted in pink.

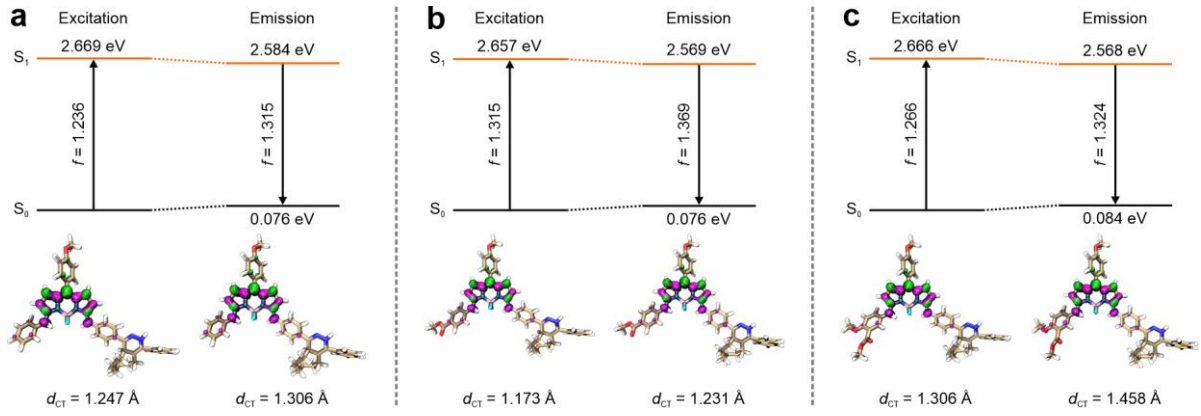

Fig. S11 Energy levels and f of key states with corresponding hole-electron distributions and d_{CT} of (a) **2a-Pz**, (b) **2b-Pz**, and (c) **2c-Pz** during the excitation and emission processes in DMSO. Electron: highlighted in green; Hole: highlighted in pink.

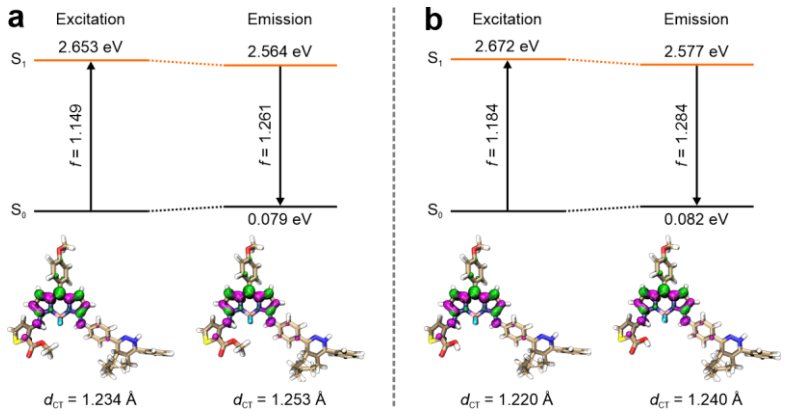

Fig. S12 Energy levels and *f* of key states with corresponding hole-electron distributions and d_{CT} of (a) **2d-Pz** and (b) **2e-Pz-Pz** during the excitation and emission processes in DMSO. Electron: highlighted in green; Hole: highlighted in pink.

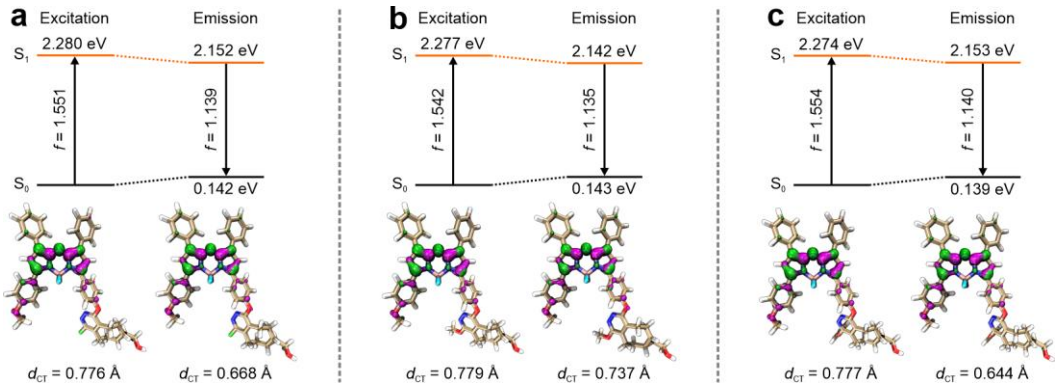

Fig. S13 Energy levels and *f* of key states with corresponding hole-electron distributions and d_{CT} of (a) **3a-Pz**, (b) **3b-Pz**, and (c) **3c-Pz** during the excitation and emission processes in water. Electron: highlighted in green; Hole: highlighted in pink.

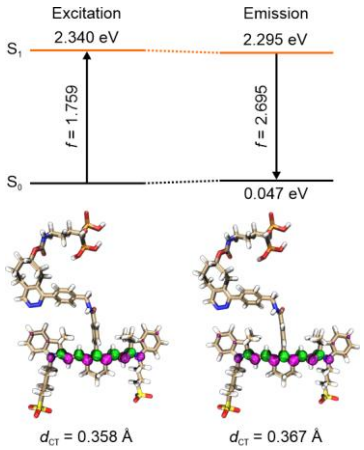

Fig. S14 Energy levels and *f* of key states with corresponding hole-electron distributions and d_{CT} of **4-Pz** during the excitation and emission processes in DMSO. Electron: highlighted in green; Hole: highlighted in pink.

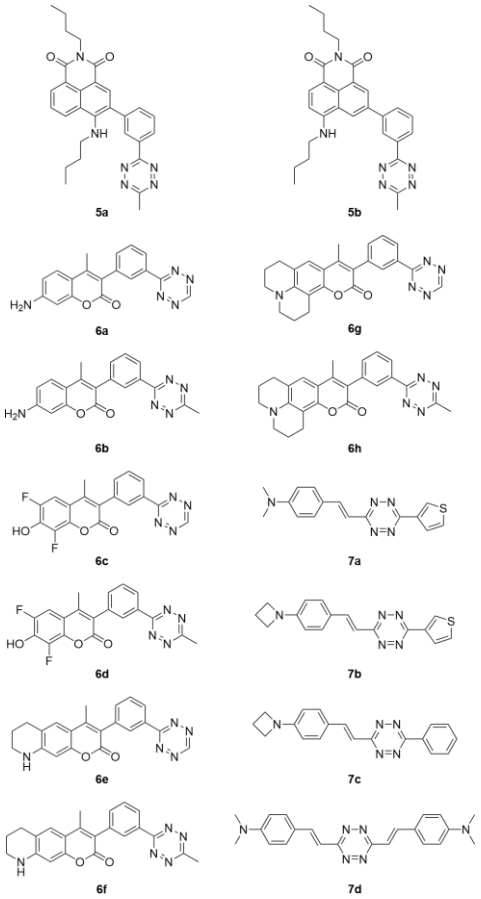

Fig. S15 Molecular structures of 14 tetrazine-based/merged fluorogenic labels with the fluorescence emissions in the visible region.

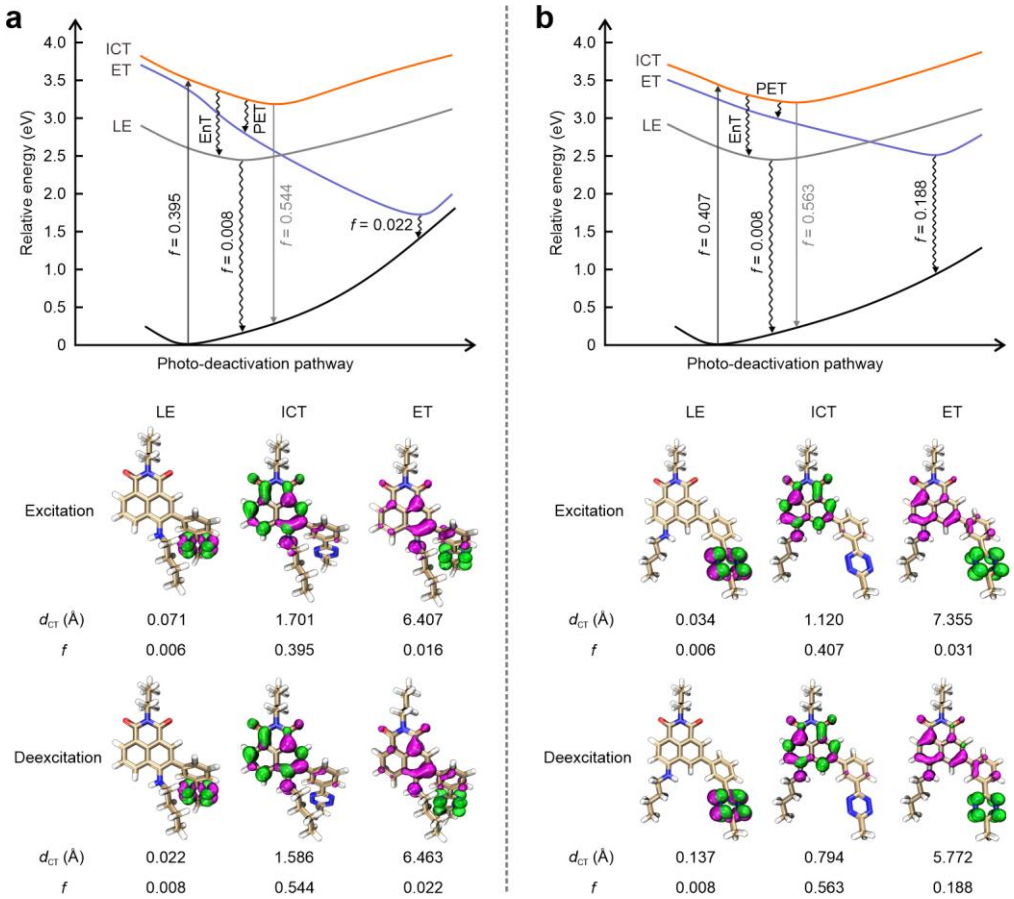

Fig. S16 Energy levels of key states with corresponding hole-electron distributions, d_{CT}, and f of (a) **5a** and (b) **5b** during the excitation and deexcitation processes in water. LE: locally excited; ICT: intramolecular charge transfer; ET: electron transfer; Electron: highlighted in green; Hole: highlighted in pink.

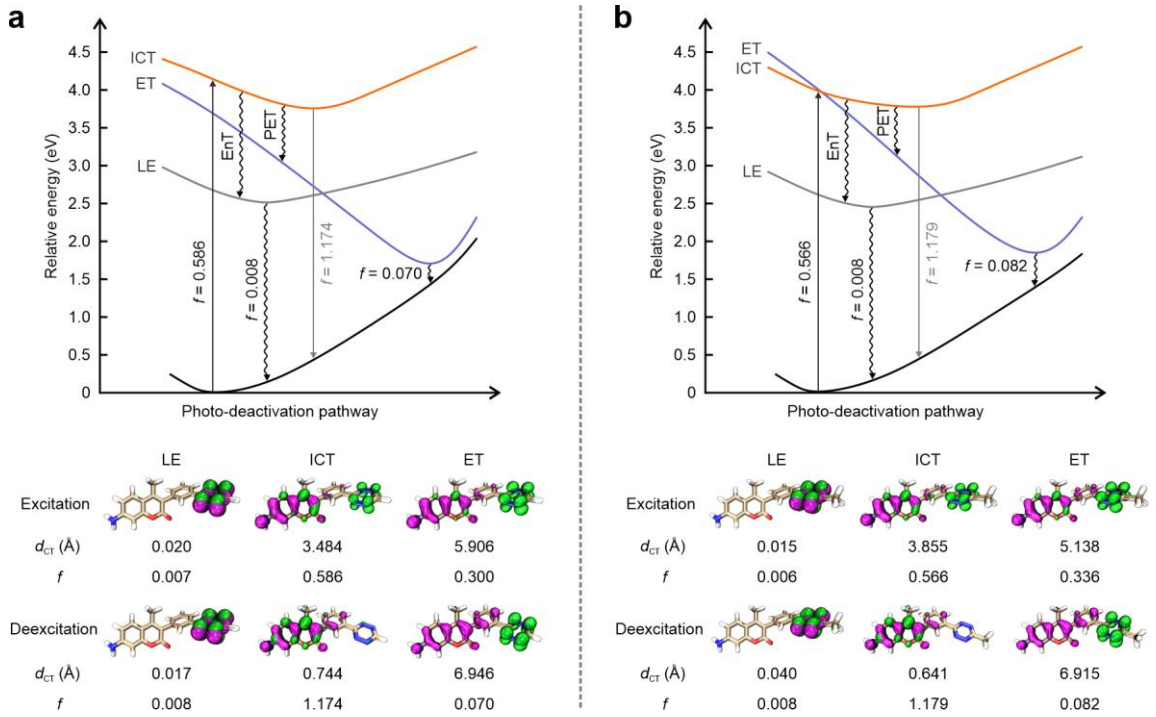

Fig. S17 Energy levels of key states with corresponding hole-electron distributions, d_{CT}, and f of (a) **6a** and (b) **6b** during the excitation and deexcitation processes in water. LE: locally excited; ICT: intramolecular charge transfer; ET: electron transfer; Electron: highlighted in green; Hole: highlighted in pink.

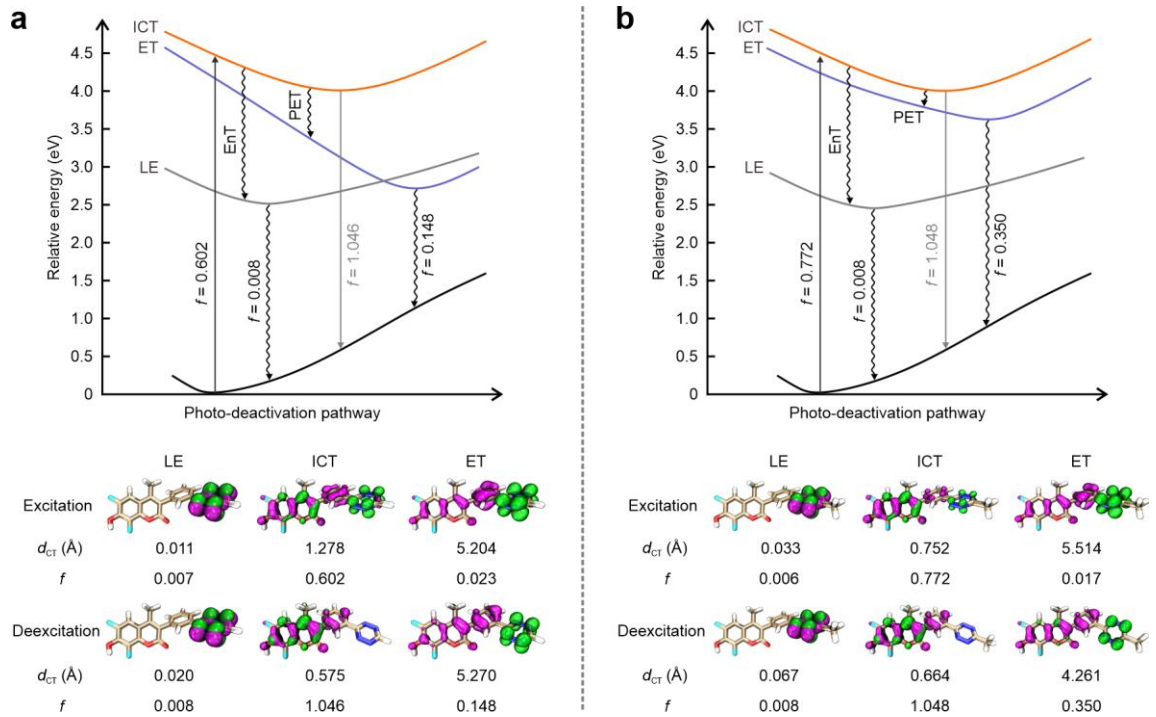

Fig. S18 Energy levels of key states with corresponding hole-electron distributions, d_{CT}, and f of (a) **6c** and (b) **6d** during the excitation and deexcitation processes in water. LE: locally excited; ICT: intramolecular charge transfer; ET: electron transfer; Electron: highlighted in green; Hole: highlighted in pink.

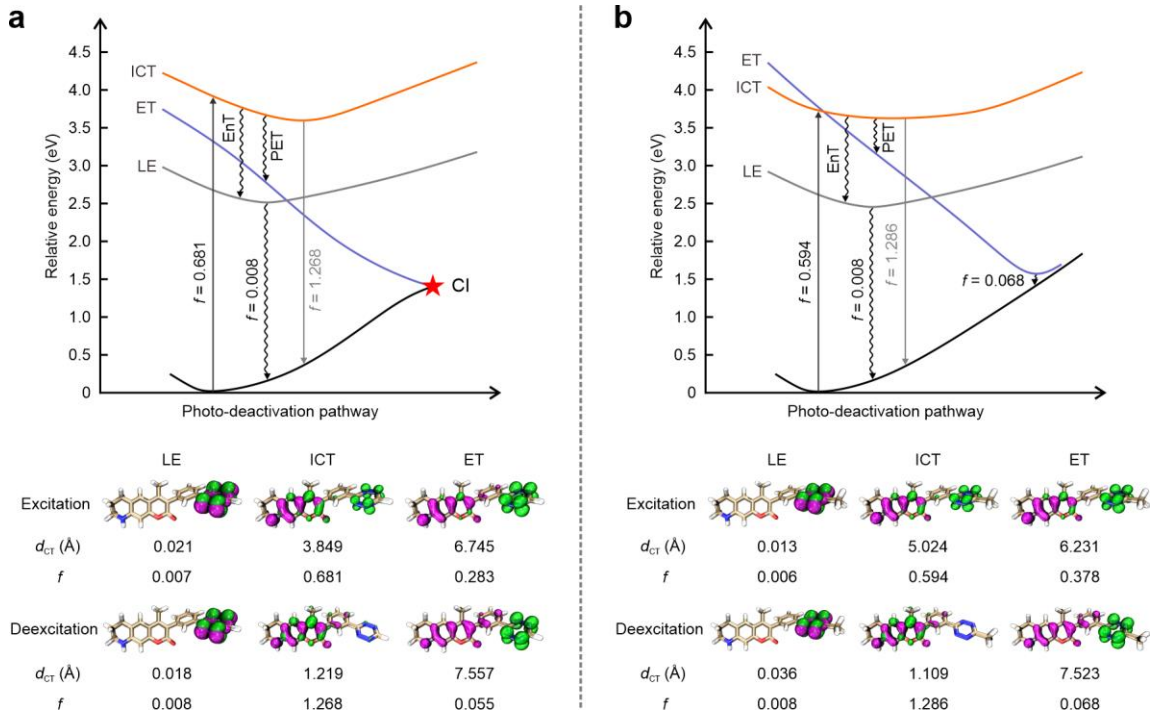

Fig. S19 Energy levels of key states with corresponding hole-electron distributions, d_{CT}, and f of (a) **6e** and (b) **6f** during the excitation and deexcitation processes in water. LE: locally excited; ICT: intramolecular charge transfer; ET: electron transfer; Electron: highlighted in green; Hole: highlighted in pink.

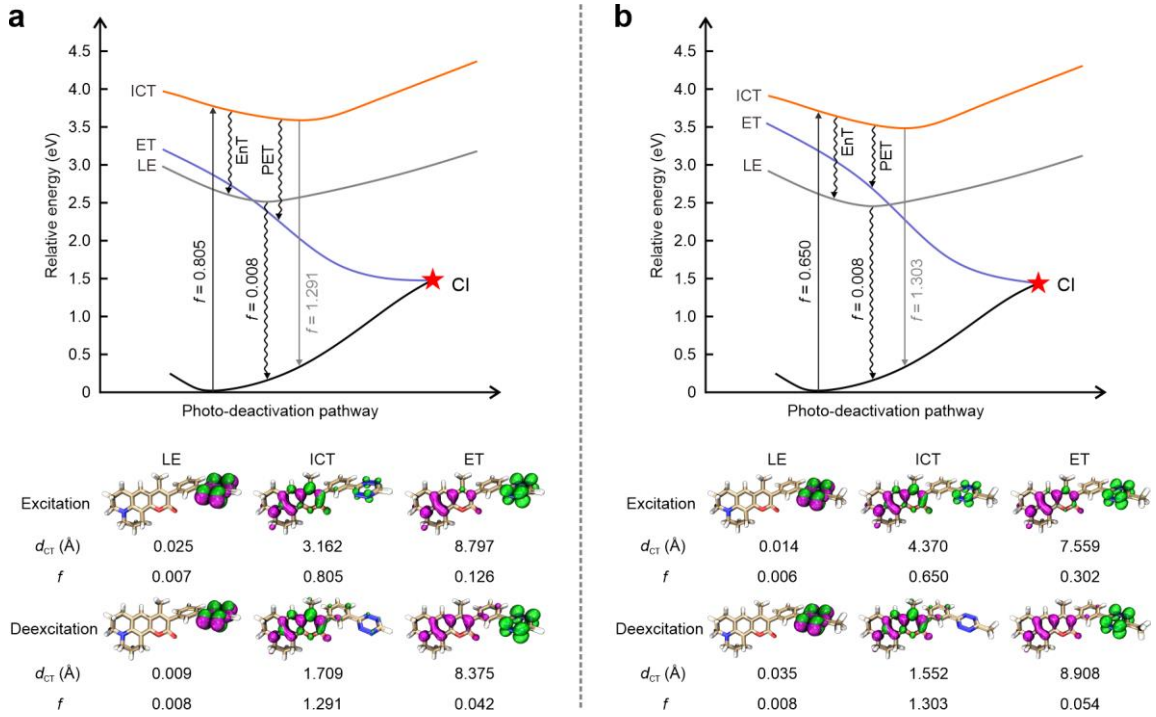

Fig. S20 Energy levels of key states with corresponding hole-electron distributions, d_{CT}, and f of (a) **6g** and (b) **6h** during the excitation and deexcitation processes in water. LE: locally excited; ICT: intramolecular charge transfer; ET: electron transfer; Electron: highlighted in green; Hole: highlighted in pink.

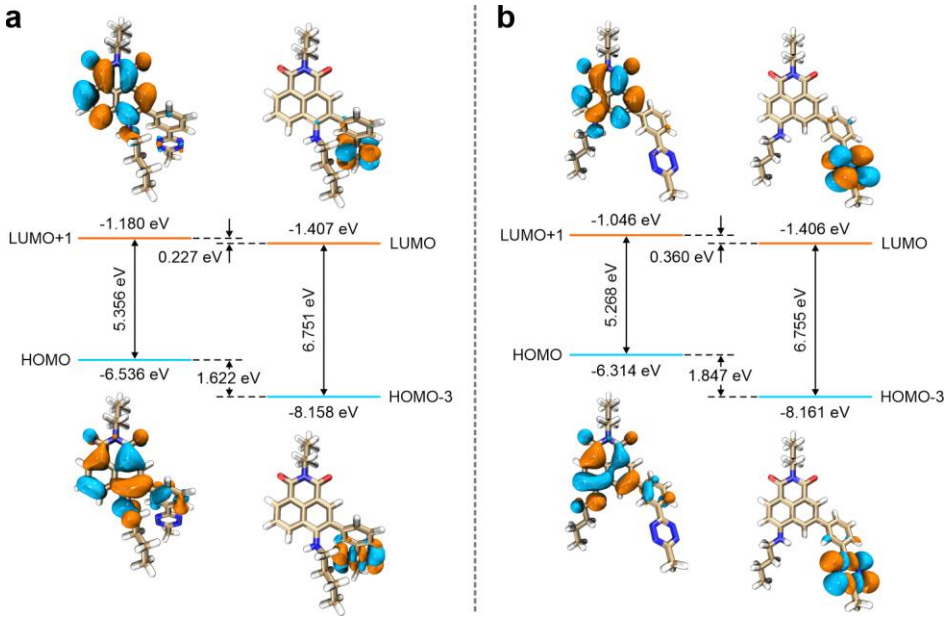

Fig. S21 Calculated electronic energies of different frontier orbitals of (a) **5a** and (b) **5b** during the vertical excitation in water.

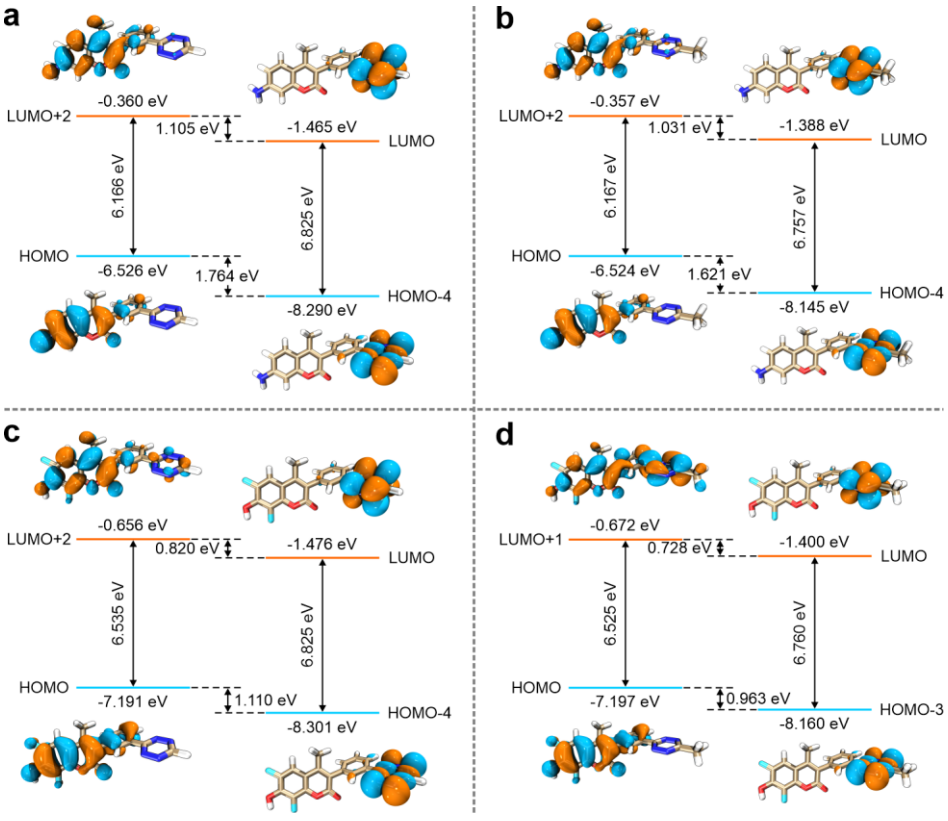

Fig. S22 Calculated electronic energies of different frontier orbitals of (a) **6a**, (b) **6b**, (c) **6c**, and (d) **6d** during the vertical excitation in water.

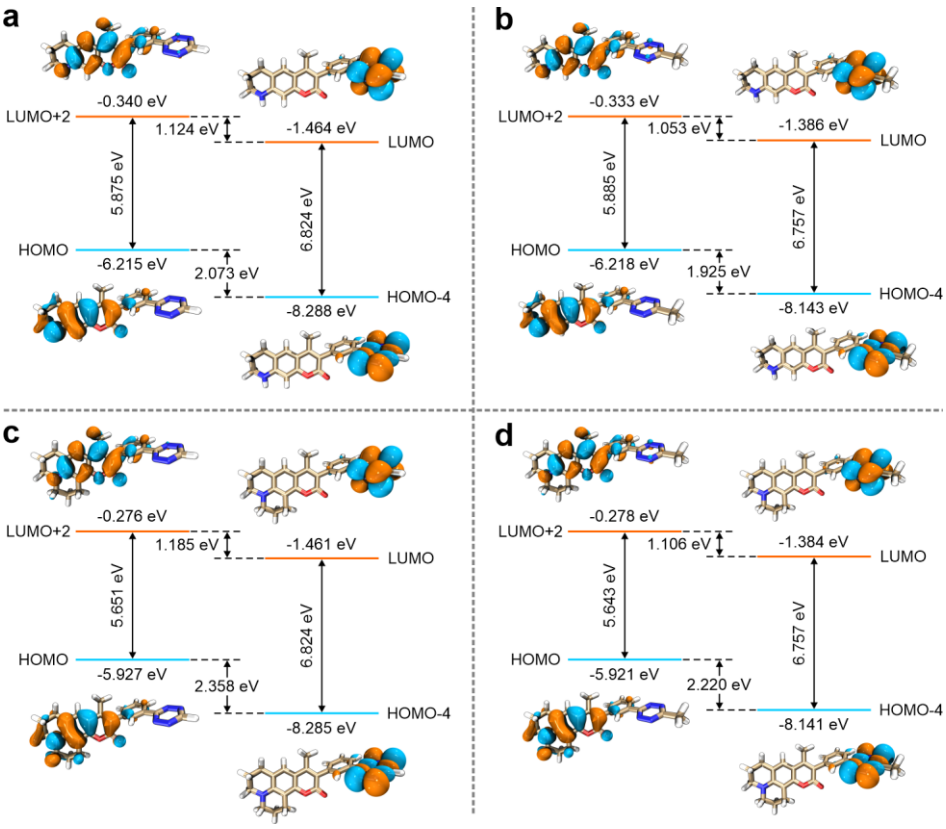

Fig. S23 Calculated electronic energies of different frontier orbitals of (a) **6e**, (b) **6f**, (c) **6g**, and (d) **6h** during the vertical excitation in water.

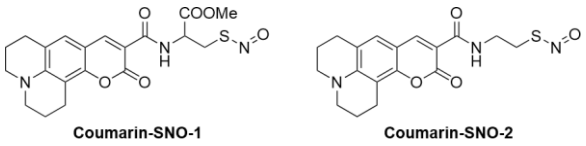

Fig. S24 Molecular structures of **Coumarin-SNO-1** (left) and **Coumarin-SNO-2** (right).

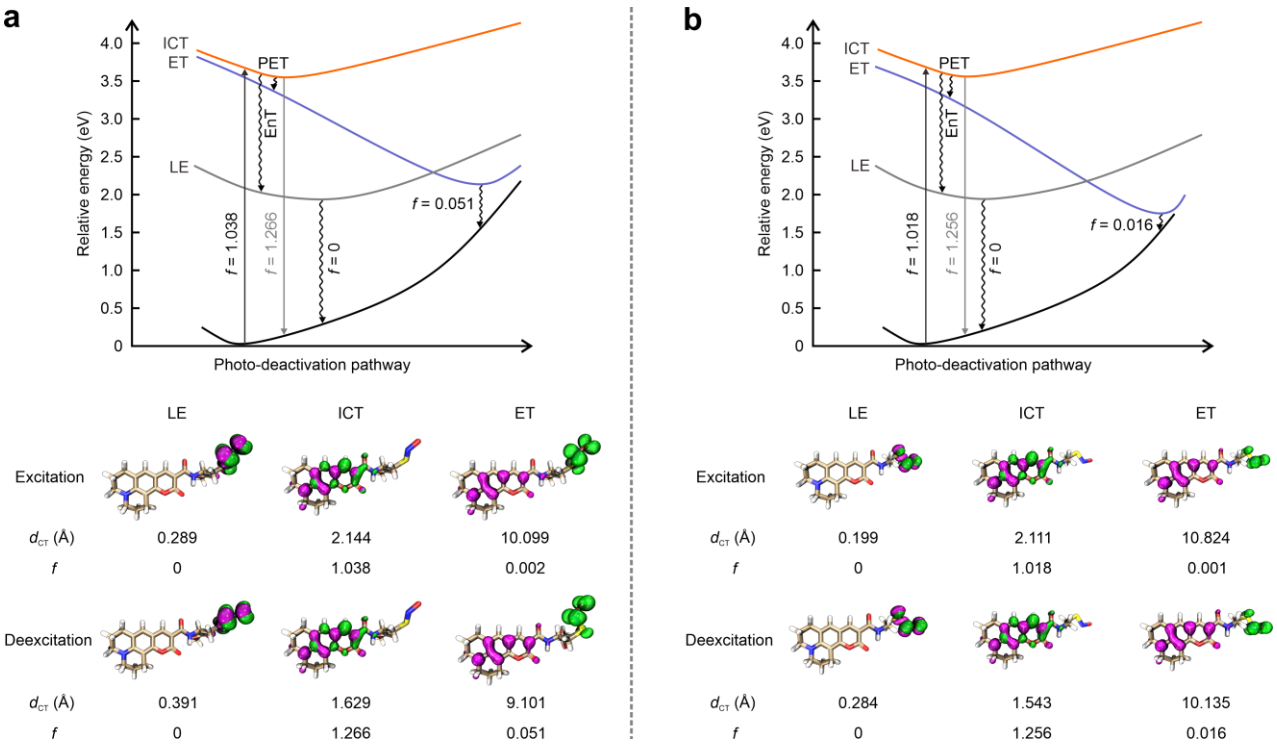

Fig. S25 Energy levels of key states with corresponding hole-electron distributions, d_{CT}, and f of (a) **Coumarin-SNO-1** and (b) **Coumarin-SNO-2** during the excitation and deexcitation processes in DMSO. LE: locally excited; ICT: intramolecular charge transfer; ET: electron transfer; Electron: highlighted in green; Hole: highlighted in pink.

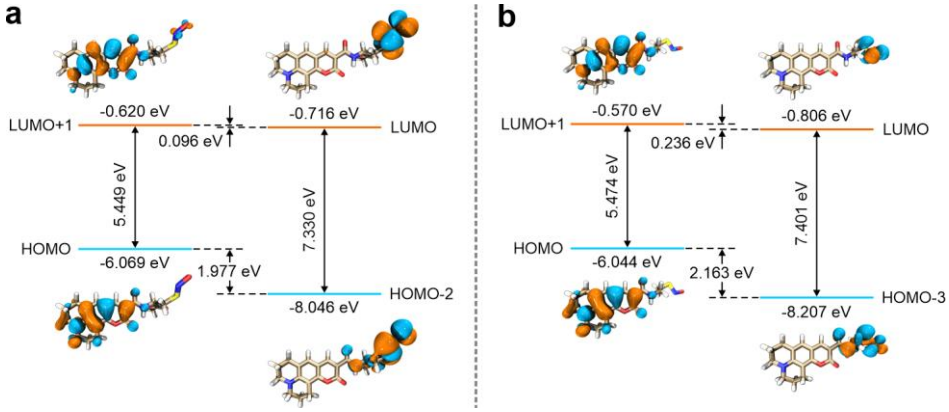

Fig. S26 Calculated electronic energies of different frontier orbitals of (a) **Coumarin-SNO-1** and (b) **Coumarin-SNO-2** during the vertical excitation in DMSO.

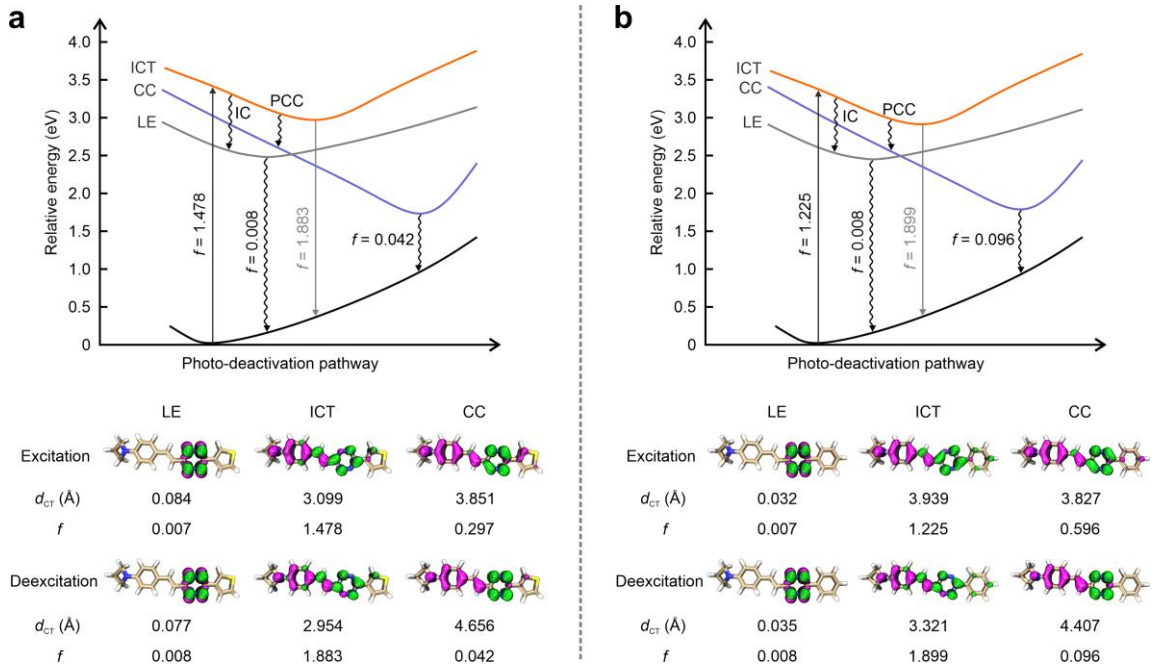

Fig. S27 Energy levels of key states with corresponding hole-electron distributions, d_{CT}, and f of (a) **7b** and (b) **7c** during the excitation and deexcitation processes in water. LE: locally excited; ICT: intramolecular charge transfer; CC: charge centralization; Electron: highlighted in green; Hole: highlighted in pink.

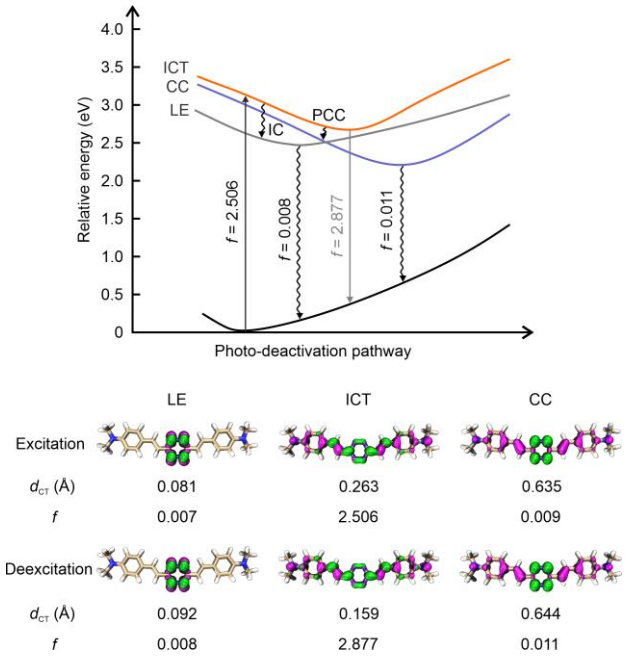

Fig. S28 Energy levels of key states with corresponding hole-electron distributions, d_{CT}, and f of **7d** during the excitation and deexcitation processes in water. LE: locally excited; ICT: intramolecular charge transfer; CC: charge centralization; Electron: highlighted in green; Hole: highlighted in pink.

Table S3 Fragment contributions (η_F, %) induced by tetrazine to the CC states in **7a-d**.

Molecule	Process	Hole	Electron	Overlap
7a	Excitation	10.11	54.04	23.38
	Deexcitation	10.38	98.36	31.95
7b	Excitation	10.40	54.44	23.79
	Deexcitation	10.32	98.43	31.87
7c	Excitation	11.31	66.20	27.36
	Deexcitation	12.64	97.29	35.07
7d	Excitation	14.83	98.87	38.29
	Deexcitation	13.06	98.99	35.96

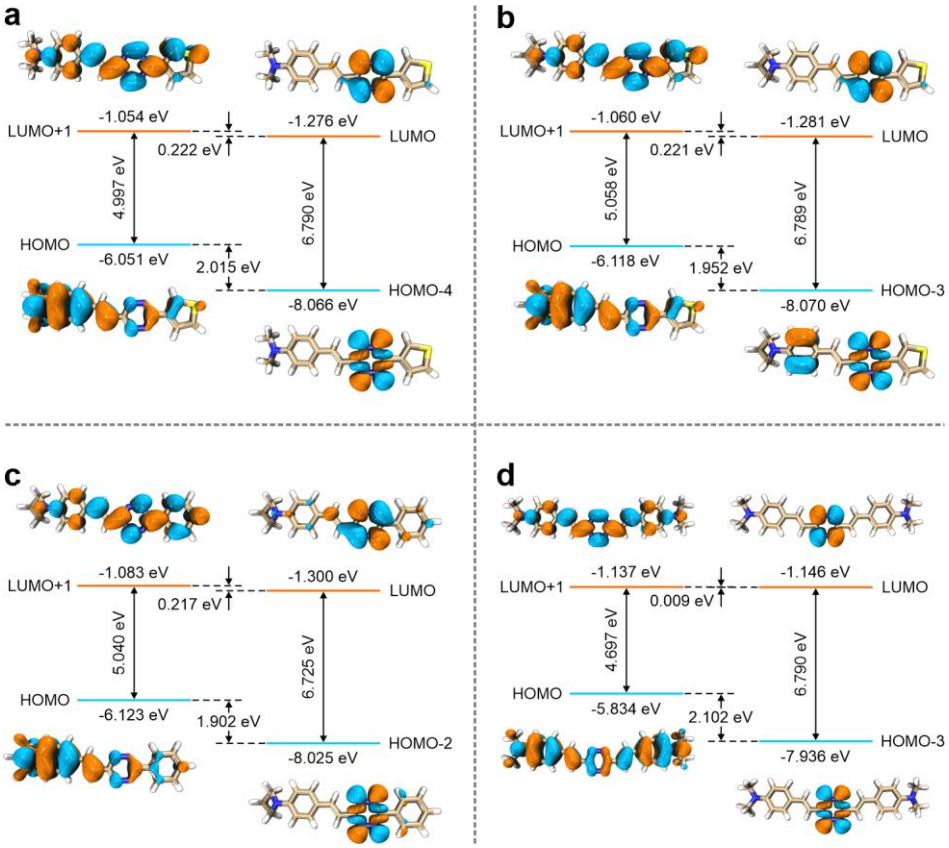

Fig. S29 Calculated electronic energies of different frontier orbitals of (a) **7a**, (b) **7b**, (c) **7c**, and (d) **7d** during the vertical excitation in water.

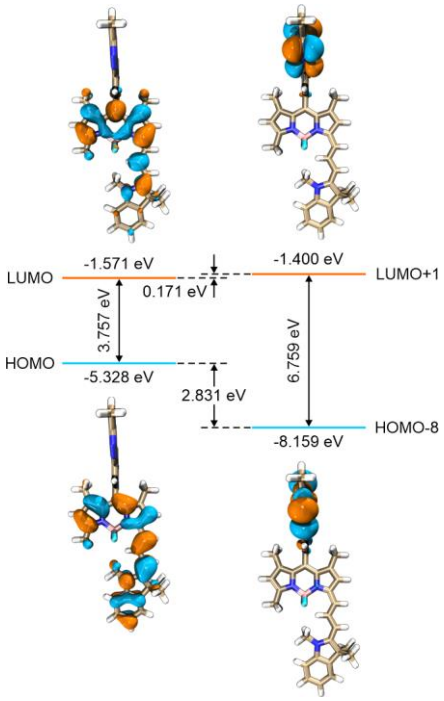

Fig. S30 Calculated electronic energies of different frontier orbitals of **1** during the vertical excitation in DMSO.

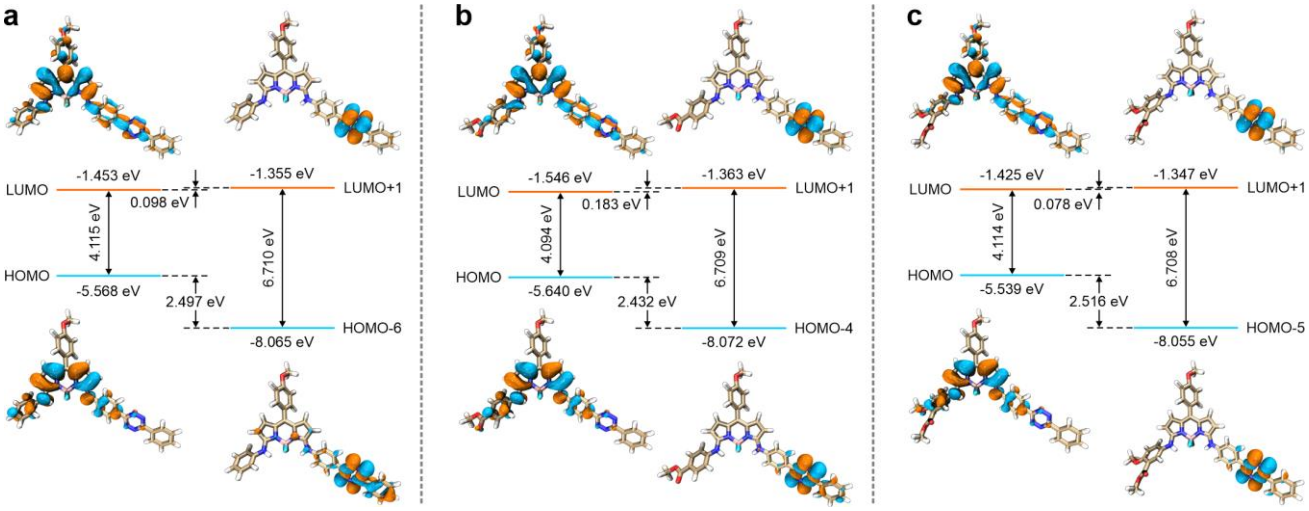

Fig. S31 Calculated electronic energies of different frontier orbitals of (a) **2a**, (b) **2b**, and (c) **2c** during the vertical excitation in DMSO.

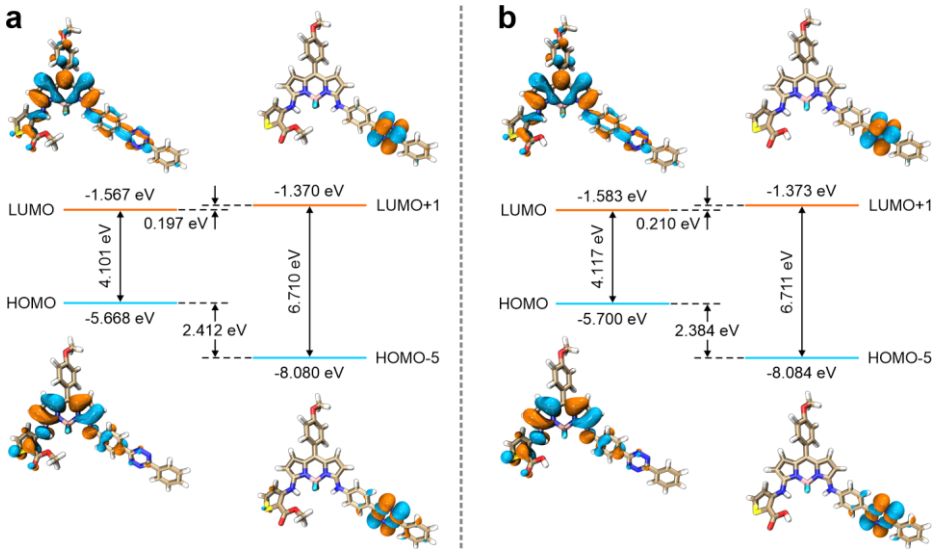

Fig. S32 Calculated electronic energies of different frontier orbitals of (a) **2d** and (b) **2e** during the vertical excitation in DMSO.

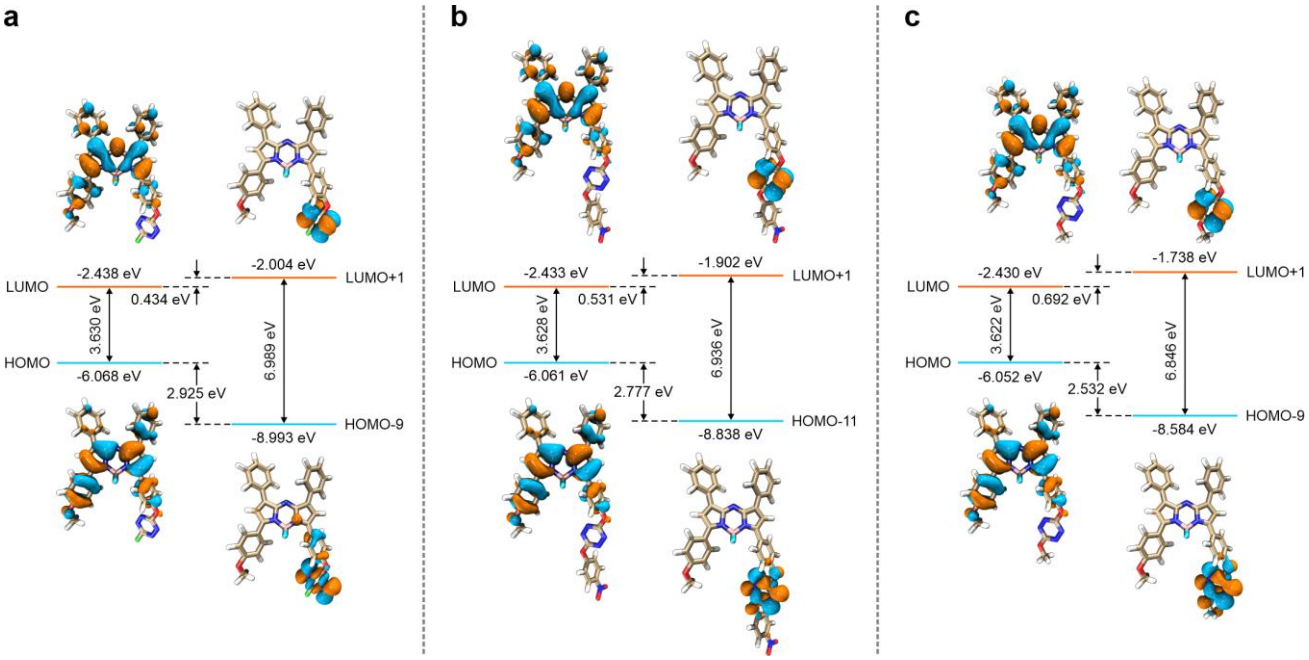

Fig. S33 Calculated electronic energies of different frontier orbitals of (a) **3a**, (b) **3b**, and (c) **3c** during the vertical excitation in water.

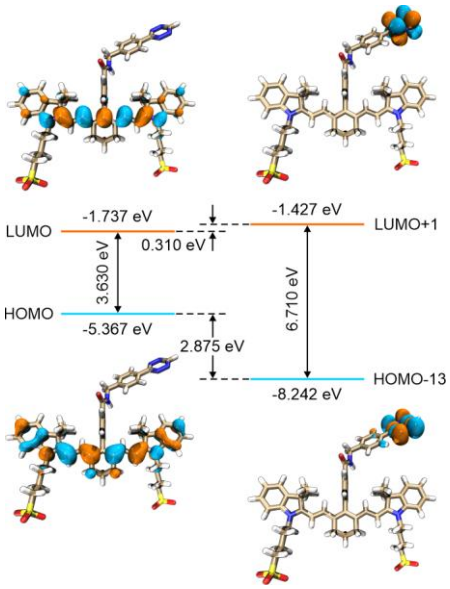

Fig. S34 Calculated electronic energies of different frontier orbitals of **4** during the vertical excitation in DMSO.

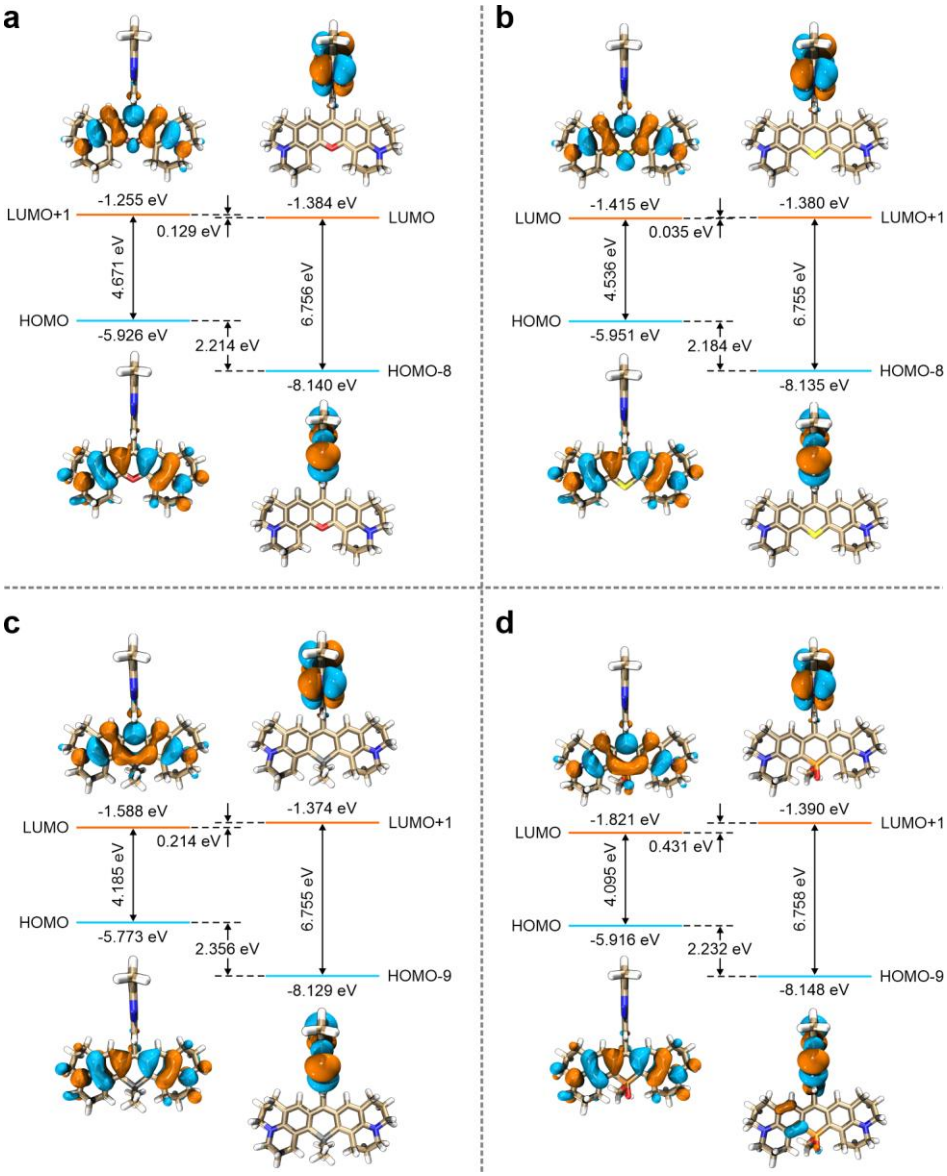

Fig. S35 Calculated electronic energies of different frontier orbitals of (a) **8a**, (b) **8b**, (c) **8c**, and (d) **8d** during the vertical excitation in DMSO.

3. References

1 Z. He, T. Ishizuka, Y. Hishikawa and Y. Xu, Click Chemistry for Fluorescence Imaging via Combination of a BODIPY-Based 'Turn-on' Probe and a Norbornene Glucosamine, *Chem. Commun.*, 2022, **58**, 12479-12482.

2 L. Chen, F. Li, Y. Li, J. Yang, Y. Li and B. He, Red-Emitting Fluorogenic BODIPY-Tetrazine Probes for Biological Imaging, *Chem. Commun.*, 2022, **58**, 298-301.

3 D. Wu and D. F. O'Shea, Fluorogenic NIR-Probes Based on 1,2,4,5-Tetrazine Substituted BF2-Azadipyrromethenes, *Chem. Commun.*, 2017, **53**, 10804-10807.

4 R. Swann, S. Slikboer, A. Genady, L. R. Silva, N. Janzen, A. Faraday, J. F. Valliant and S. Sadeghi, Tetrazine-Derived Near-Infrared Dye for Targeted Photoacoustic Imaging of Bone, *J. Med. Chem.*, 2023, **66**, 6025-6036.

5 A. D. Becke, Density-Functional Thermochemistry. III. The Role of Exact Exchange, *J Chem. Phys.*, 1993, **98**, 5648-5652.

6 G. Scalmani, M. J. Frisch, B. Mennucci, J. Tomasi, R. Cammi and V. Barone, Geometries and Properties of Excited States in the Gas Phase and in Solution: Theory and Application of a Time-Dependent Density Functional Theory Polarizable Continuum Model, *J. Chem. Phys.*, 2006, **124**, 94107.

7 M. J. Frisch, G. W. Trucks, H. B. Schlegel, G. E. Scuseria, M. A. Robb, J. R. Cheeseman, G. Scalmani, V. Barone, G. A. Petersson, H. Nakatsuji, X. Li, M. Caricato, A. V. Marenich, J. Bloino, B. G. Janesko, R. Gomperts, B. Mennucci, H. P. Hratchian, J. V. Ortiz, A. F. Izmaylov, J. L. Sonnenberg, D. WilliamsYoung, F. Ding, F. Lipparini, F. Egidi, J. Goings, B. Peng, A. Petrone, T. Henderson, D. Ranasinghe, V. G. Zakrzewski, J. Gao, N. Rega, G. Zheng, W. Liang, M. Hada, M. Ehara, K. Toyota, R. Fukuda, J. Hasegawa, M. Ishida, T. Nakajima, Y. Honda, O. Kitao, H. Nakai, T. Vreven, K. Throssell, J. A. Montgomery, Jr., J. E. Peralta, F. Ogliaro, M. J. Bearpark, J. J. Heyd, E. N. Brothers, K. N. Kudin, V. N. Staroverov, T. A. Keith, R. Kobayashi, J. Normand, K. Raghavachari, A. P. Rendell, J. C. Burant, S. S. Iyengar, J. Tomasi, M. Cossi, J. M. Millam, M. Klene, C. Adamo, R. Cammi, J. W. Ochterski, R. L. Martin, K. Morokuma, O. Farkas, J. B. Foresman, and D. J. Fox, Gaussian, Inc., Wallingford CT, 2016.

8 A. D. Becke, A New Mixing of Hartree–Fock and Local Density–Functional Theories, *J. Chem. Phys.*, 1993, **98**, 1372-1377.

9 G. A. Petersson, A. Bennett, T. G. Tensfeldt, M. A. Al–Laham, W. A. Shirley and J. Mantzaris, A Complete Basis Set Model Chemistry. I. The Total Energies of Closed–Shell Atoms and Hydrides of the First-Row Elements, *J. Chem. Phys.*, 1988, **89**, 2193-2218.

10 G. Petersson and M. A. Al–Laham, A Complete Basis Set Model Chemistry. II. Open–Shell Systems and the Total Energies of the First–Row Atoms, *J. Chem. Phys.*, 1991, **94**, 6081-6090.

11 A. V. Marenich, C. J. Cramer and D. G. Truhlar, Universal Solvation Model Based on Solute Electron Density and on a Continuum Model of the Solvent Defined by the Bulk Dielectric Constant and Atomic Surface Tensions, *J. Phys. Chem. B*, 2009, **113**, 6378-6396.

12 M. Caricato, B. Mennucci, J. Tomasi, F. Ingrosso, R. Cammi, S. Corni and G. Scalmani, Formation and Relaxation of Excited States in Solution: A New Time Dependent Polarizable Continuum Model Based on Time Dependent Density Functional Theory, *J. Chem. Phys.*, 2006, **124**, 124520.

13 T. Lu and F. Chen, Multiwfn: A Multifunctional Wavefunction Analyzer, *J. Comput Chem.*, 2012, **33**, 580-592.

14 W. Humphrey, A. Dalke and K. Schulten, VMD: Visual Molecular Dynamics, *J. Mol. Graph.*, 1996, **14**, 33-38.